JOURNAL OF THE ROYAL SOCIETY Interface

Hydrodynamics of sailing of the Portuguese man-of-war *Physalia physalis*

G. Iosilevskii and D. Weihs

J. R. Soc. Interface 2009 **6**, 613-626 first published online 15 December 2008
doi: 10.1098/rsif.2008.0457

JOURNAL OF THE ROYAL SOCIETY Interface

J. R. Soc. Interface (2009) **6**, 613–626
doi:10.1098/rsif.2008.0457
Published online 15 December 2008

Hydrodynamics of sailing of the Portuguese man-of-war *Physalia physalis*

G. Iosilevskii* and D. Weihs

Faculty of Aerospace Engineering, Technion, Haifa 32000, Israel

Physalia physalis, commonly known as the Portuguese man-of-war (PMW), is a peculiar looking colony of specialized polyps. The most conspicuous members of this colony are the gas-filled sail-like float and the long tentacles, budding asymmetrically beneath the float. This study addresses the sailing of the PMW, and, in particular, the hydrodynamics of its trailing tentacles, the interaction between the tentacles and the float and the actual sailing performance. This paper attempts to provide answers for two of the many open questions concerning *P. physalis*: why does it need a sail? and how does it harness the sail?

Keywords: *Physalia physalis*; Portuguese man-of-war; hydrodynamics of sailing; slender body theory

1. INTRODUCTION

Physalia physalis (phylum: Cnidaria, class: Hydrozoa, order: Siphonophora, family: Physaliidae), also known as the Portuguese man-of-war (PMW for short) or the blue bottle, is a colony of numerous polyps (Totton & Mackie 1960; Bardi & Marques 2007). One of these polyps develops into a gas-filled float that looks like a sail (pneumatophore); others develop into digesting polyps (gastrozooids), reproductive polyps (gonozooids) and long hunting tentacles (dactylozooids). The float is asymmetric, with tentacles budding off-centre on approximately half of its length (figure 1). The population of the PMW is divided between those having their tentacles to the right of the sail and sailing on the starboard tack, and those having their tentacles to the left of sail and sailing on the port tack. Hydrodynamic aspects of the PMW sailing are the subject matter of this study.

To avoid ambiguity, this is perhaps the right place to define what 'left' and 'right' directions are for the PMW. To this end, consider a PMW sailing as in figure 2*a*. Were this PMW a sail boat rigged only with a mainsail, its sailing posture could have been replicated either by heading close to the wind and drifting downwind (figure 2*b*), or by sailing on a broad reach (figure 2*c*). In the first case, the sail boat is trimmed with the sail sheeted in, and a sea anchor attached to its left side, near the mast. In the second case, the sail boat is trimmed with the sail sheeted out towards the bow, and possibly no anchor at all. This sail position is rather unusual for a sail boat (it may even be inadmissible mechanically), but can be easily demonstrated on a sailboard. We believe that the first case better represents the sailing PMW, mainly because of its sail orientation relative to the body. Hence, we place the bow of the PMW at its oral end, where the tentacles are, inferring fore and aft directions accordingly. Left and right directions will be defined as if standing on the vessel and facing the bow. Thus, the PMW depicted in figure 2*a* has the sail on its right and the tentacles on its left. Totton & Mackie (1960, p. 316) defined this configuration as 'right-handed'.

When addressing the hydrodynamics of the sailing of the PMW one cannot avoid mentioning another natural sailor, *Velella velella* (Francis 1991). The two are comparably rigged, but have very different underwater parts reflecting their feeding strategies. The PMW has a few very long tentacles that slowly drag behind the animal deep below the water surface; *V. velella* has many short tentacles that apparently work as a rake, collecting food from the water surface as the animal skims along. Although it is possible that the two have developed comparable mechanisms to harness their sails, they certainly deserve separate studies. This study is concerned with the PMW only.

2. A TRAILING TENTACLE

Consider a single tentacle of length l and uniform diameter d trailing through the water by being pulled horizontally with constant velocity v at its upper end. The forces acting on the trailing tentacle can be associated with gravity and its motion. The forces associated with gravity are given by

$$F_g = \frac{\pi}{4}(\rho_t - \rho) d^2 g l, \tag{2.1}$$

where ρ_t, ρ and g are the density of the tentacle, the density of water and the acceleration of gravity, respectively. The forces associated with the motion can be separated into tangential and normal components, which are assumed to be given, per unit length of a tentacle, by the constitutive relations

*Author for correspondence (igil@aerodyne.technion.ac.il).

Received 25 October 2008
Accepted 17 November 2008

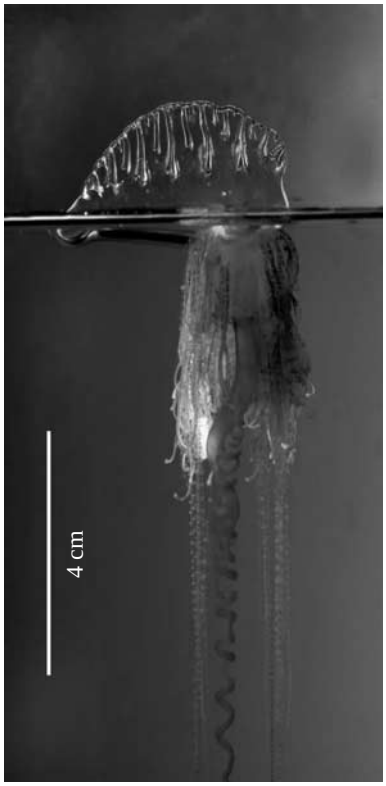

Figure 1. *P. physalis*. Photograph by A. E. Migotto, Center of Marine Biology, University of Sao Paulo, Brazil.

$$f_{\mathrm{t}} = \frac{1}{2}\rho v_{\mathrm{t}}^2 d C_{\mathrm{D,t}}, \quad f_{\mathrm{n}} = \frac{1}{2}\rho v_{\mathrm{n}}^2 d C_{\mathrm{D,n}}, \tag{2.2}$$

where $C_{\mathrm{D,t}}$ and $C_{\mathrm{D,n}}$ are the drag coefficients of the tentacle in axial flow and cross-flow, whereas v_{t} and v_{n} are the respective velocity components. $C_{\mathrm{D,t}}$ and $C_{\mathrm{D,n}}$ are estimated in appendix A as approximately 0.01 and approximately 1, respectively; $\rho_{\mathrm{t}} - \rho$ is estimated as a few hundredths of ρ.

It is shown in appendix B that under the influence of these forces the trailing tentacle remains straight. Its angle with the vertical,

$$\theta = \arcsin\left(\frac{-1+\sqrt{1+4P^2}}{2P}\right), \tag{2.3}$$

is governed by a single dimensionless parameter,

$$P = \frac{\rho}{\rho_{\mathrm{t}} - \rho}\frac{2C_{\mathrm{D,n}}v^2}{\pi g d}, \tag{2.4}$$

representing the ratio of hydrodynamic to gravity forces (see (B 21) and (B 6)).[1] The dependence of θ on P is depicted in figure 3*a*. With, say, $P<10$, minute variations in density, diameter or drag coefficient among the tentacles should cause them to spread fan-like under the float, with tentacles with smaller P hanging at lower angles to the vertical.

[1]Sin θ can be identified with $x_{s,}$ used in appendix B; P can be identified with the product $pC_{\mathrm{D,n}}$.

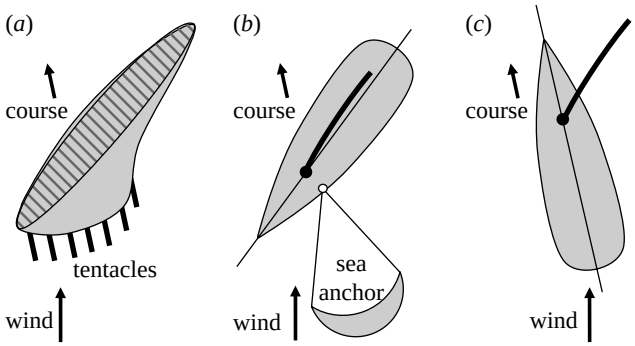

Figure 2. (*a*) Top view of a right-handed PMW sailing on the port tack, (*b*) a sail boat drifting with a sea anchor and (*c*) a sail boat on a broad reach.

The force T needed to pull a tentacle is

$$\begin{aligned} T &= F_{\mathrm{g}}\left(P\frac{C_{\mathrm{D,t}}}{C_{\mathrm{D,n}}}\sin^2\theta + \cos\theta\right) \\ &= F_{\mathrm{g}}\left(P\frac{C_{\mathrm{D,t}}}{C_{\mathrm{D,n}}}\left(\frac{-1+\sqrt{1+4P^2}}{2P}\right)^2\right. \\ &\quad \left. + \frac{1}{\sqrt{P}}\left(\frac{-1+\sqrt{1+4P^2}}{2P}\right)^{1/2}\right); \end{aligned} \tag{2.5}$$

adjusting the notation with appendix B, this equation immediately follows (B 22). T is depicted in figure 3 together with its horizontal,

$$F_X = T\sin\theta, \tag{2.6}$$

and vertical,

$$F_Y = T\cos\theta, \tag{2.7}$$

components.

It is evident from figure 3*b* that the force acting on a trailing tentacle initially decreases with the trailing velocity. In fact, for small values of P, equations (2.3) and (2.5)–(2.7) yield

$$\theta = P - \frac{5}{6}P^3 + \cdots, \tag{2.8a}$$

$$\frac{T}{F_{\mathrm{g}}} = 1 - \frac{1}{2}P^2 + \cdots, \tag{2.8b}$$

$$\frac{F_X}{F_{\mathrm{g}}} = P - \frac{3}{2}P^3 + \cdots, \tag{2.8c}$$

$$\frac{F_Y}{F_{\mathrm{g}}} = 1 - P^2 + \cdots. \tag{2.8d}$$

An increase in trailing velocity sweeps the tentacle back (2.8*a*), increasing the vertical force component, and hence decreasing the effective 'weight' of the tentacle in the water (2.8*d*). Since the angle of the tentacle with the vertical is still small at this stage, the total force on the tentacle decreases as well (2.8*b*), in spite of the increase in the horizontal force component (2.8*c*).

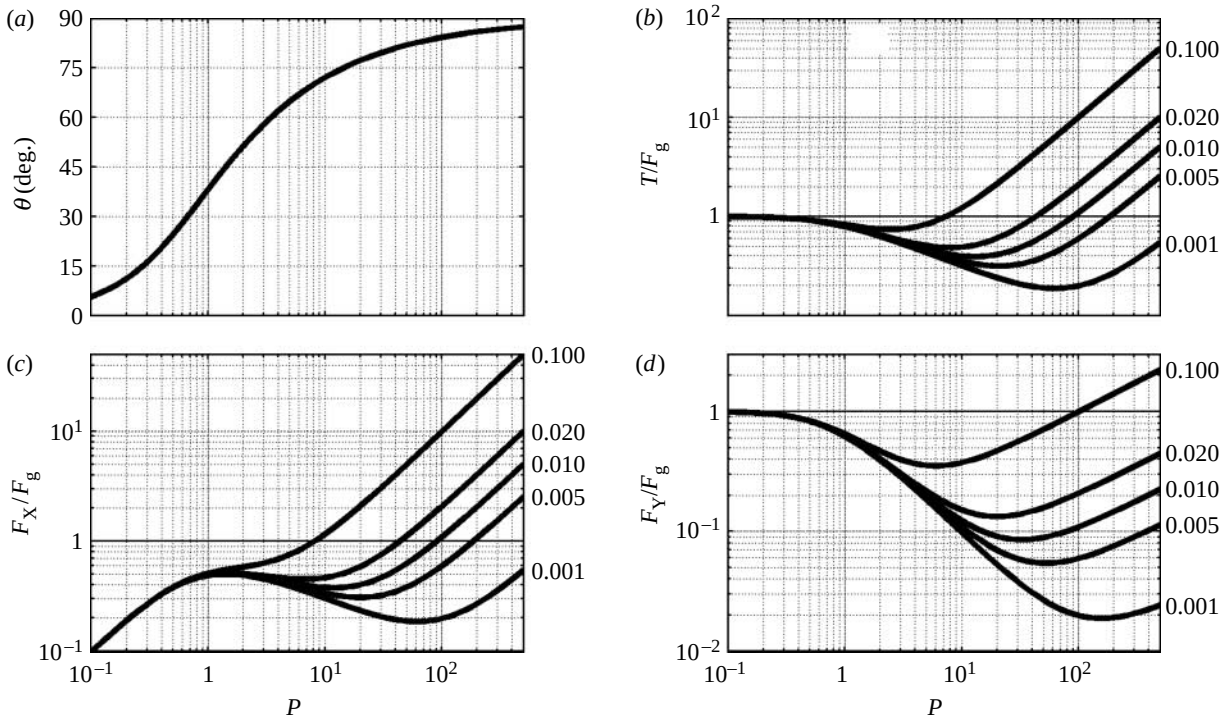

Figure 3. (*a*) The angle of the tentacle from vertical, (*b*) the total force needed to drag the tentacle and (*c*) the horizontal and (*d*) vertical components of that force. Numbers appearing to the right of the respective curves mark the $C_{\mathrm{D,t}}/C_{\mathrm{D,n}}$ values.

For very large values of P, the tentacle becomes almost horizontal, with

$$\theta = \frac{\pi}{2} - \frac{1}{\sqrt{P}} + \cdots, \tag{2.9a}$$

and, from that point on, an increase in trailing velocity increases the forces on the tentacle. Explicitly, for large P,[2]

$$\frac{T}{F_{\mathrm{g}}} = P\,\frac{C_{\mathrm{D,t}}}{C_{\mathrm{D,n}}} + \frac{1}{\sqrt{P}} + \cdots, \tag{2.9b}$$

$$\frac{F_X}{F_{\mathrm{g}}} = P\,\frac{C_{\mathrm{D,t}}}{C_{\mathrm{D,n}}} + \frac{1}{\sqrt{P}} + \cdots, \tag{2.9c}$$

$$\frac{F_Y}{F_{\mathrm{g}}} = \sqrt{P}\,\frac{C_{\mathrm{D,t}}}{C_{\mathrm{D,n}}} + \frac{1}{P} + \cdots. \tag{2.9d}$$

In the intermediate range of P, there is a noticeable drop in the horizontal force F_X acting on the tentacle when $C_{\mathrm{D,t}}/C_{\mathrm{D,n}}$ is smaller than, say, a few hundredths (figure 3*c*). At this range of P, an increase in the trailing velocity sweeps the tentacle sufficiently back to reduce the cross-flow velocity on the tentacle. Since the associated increase in the axial velocity may carry only a limited drag penalty when $C_{\mathrm{D,t}}/C_{\mathrm{D,n}}$ is small, there exists a certain range of trailing velocities where the horizontal force component decreases with increasing trailing velocity. For a typical tentacle of the PMW, the ratio $C_{\mathrm{D,t}}/C_{\mathrm{D,n}}$ is approximately 0.01 (appendix A), and, therefore, the decrease in the horizontal force component is expected for, say, $1<P<10$.

Curling a tentacle increases its effective diameter and hence decreases the effective value of P. This obviously puts the tentacle at a smaller angle to the vertical (figure 3*a*) and reduces tension when P is large (figure 3*b*). Reports that the tentacles curl up when provoked (Totton & Mackie 1960, p. 376) suggest the possibility that the PMW may intentionally curl a tentacle when the tension in it crosses a certain threshold.

Using (2.3)–(2.5) and (2.1), equation (2.6) for the horizontal force component can be recast as

$$F_X = \frac{1}{2}\rho v^2 dl C_{\mathrm{H,t}}, \tag{2.10}$$

where

$$C_{\mathrm{H,t}} = C_{\mathrm{D,t}}\left(\frac{-1+\sqrt{1+4P^2}}{2P}\right)^3 + C_{\mathrm{D,n}}\left(\frac{-1+\sqrt{1+4P^2}}{2P^2}\right)^{3/2}. \tag{2.11}$$

$C_{\mathrm{H,t}}$ can be interpreted as the effective drag coefficient of the tentacle; it equals $C_{\mathrm{D,n}}$ when P is small and the tentacle is almost vertical, and $C_{\mathrm{D,t}}$ when P is large and the tentacle is almost horizontal (figure 4).

3. TRIMMING THE SAIL

The force exerted on a body moving relative to a fluid can be loosely separated into lift and drag components; the former perpendicular to the direction of the flow as seen from the body, and the latter parallel to it. In order

[2]This is not a formal expansion—it includes the leading order term (with respect to P) containing the ratio $C_{\mathrm{D,t}}/C_{\mathrm{D,n}}$, and the leading order term which is independent of it.

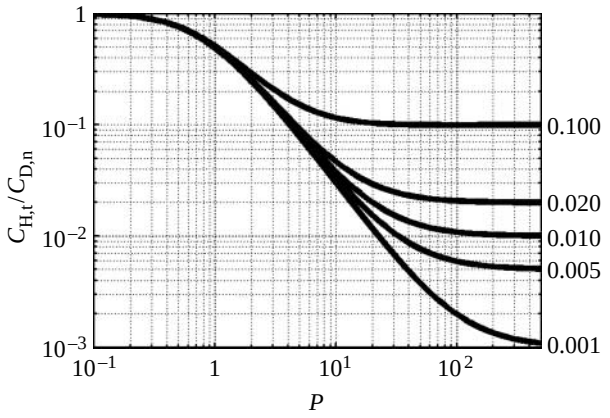

Figure 4. Effective drag coefficient of a tentacle. Numbers appearing to the right of the respective curves mark the $C_{\mathrm{D,t}}/C_{\mathrm{D,n}}$ values.

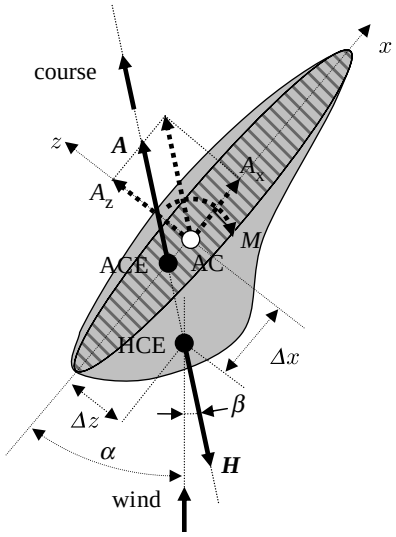

Figure 5. Top view of the balance of forces for a right-handed PMW sailing on the port tack. The sail (cross-hatched) is set at the angle α to the wind; the PMW sails at angle β from downwind. The hydrodynamic force $\boldsymbol{H}$ is counterbalanced by the aerodynamic force $\boldsymbol{A}$. The forces act at the respective centres of effort, HCE and ACE. The aerodynamic forces associated with the aerodynamic centre (AC) appear as dotted lines.

to produce lift, the body has to be asymmetric with respect to that direction. Typically, this implies setting the body at an angle with the direction of the flow; this angle is generally referred to as the angle of attack. Indeed, in light winds, the PMW balances (trims) itself at the angle of attack of approximately 40° (Totton & Mackie 1960, p. 322). The possible ways the PMW does that are considered below.

3.1. Balance of forces in the horizontal plane

A schematic balance of forces in the horizontal plane is shown in figure 5. The hydrodynamic forces on the submerged part of the PMW are assumed to provide drag only and hence act in the direction opposing the direction of sailing. By definition, a point exists where these forces produce no couple. This point is called the centre of effort; it is marked 'HCE' in figure 5. The aerodynamic forces are generally not aligned with the wind direction, but can be associated with the respective centre of effort as well; it is marked 'ACE' in figure 5. In equilibrium, i.e. when the PMW is moving at a constant velocity, the aerodynamic forces are counterbalanced by the hydrodynamic forces, implying that the two are equal in magnitude and oppose each other.

The location of the centre of effort of an asymmetric lift-producing body is known to move considerably as the angle of attack changes (this result is recapitulated in appendix C—see equation (C 27) thereat). In those cases, it is more convenient to use the notion of the aerodynamic centre—a geometric point where the couple remains independent of the angle of attack (Bisplinghoff *et al.* 1996, p. 219); it is marked 'AC' in figure 5. The location of the aerodynamic centre is known to be practically fixed (see equation (C 28) in appendix C).

Referring to figure 5, the equilibrium conditions about the hydrodynamic centre of effort (HCE) can be written as

$$A_x - H\cos(\alpha+\beta) = 0, \tag{3.1a}$$

$$A_z - H\sin(\alpha+\beta) = 0 \tag{3.1b}$$

and

$$M - A_z\Delta x + A_x\Delta z = 0, \tag{3.1c}$$

where A_x and A_z are the components of the aerodynamic force along the respective axes; M is the (aerodynamic) couple about the aerodynamic centre; H is the hydrodynamic force; α is the angle of attack; β is the angle between the direction of sailing and the downwind direction; and Δx and Δz are the respective distances between the aerodynamic centre of the sail and the centre of effort of the hydrodynamic forces. The associated right-handed reference frame has its x-axis horizontal, connecting the leading and trailing edges of the sail, and its z-axis horizontal and pointing to leeward.

The sailing speed v of the PMW (which is a few tens of centimetres per second) is small when compared with the wind speed U (which is a few metres per second), and hence the wind speed relative to the sail is practically U. Accordingly, the forces on the PMW can be conveniently represented by

$$A_x = \frac{1}{2}\rho_{\mathrm{A}} U^2 S_{\mathrm{A}} C_x, \tag{3.2a}$$

$$A_z = \frac{1}{2}\rho_{\mathrm{A}} U^2 S_{\mathrm{A}} C_z, \tag{3.2b}$$

$$M = \frac{1}{2}\rho_{\mathrm{A}} U^2 S_{\mathrm{A}} c_{\mathrm{A}} C_{\mathrm{M}} \tag{3.2c}$$

and

$$H = \frac{1}{2}\rho v^2 S_{\mathrm{H}} C_{\mathrm{H}}, \tag{3.2d}$$

where ρ_{A} is the density of the air; S_{A} and c_{A} are the area and the chord of the sail; S_{H} is an arbitrary reference area (e.g. the combined surface area of the tentacles);

C_x, C_z and C_M are the respective force and moment coefficients; and C_H is the hydrodynamic drag coefficient. With these, equilibrium conditions (3.1*a*)–(3.1*c*) take on the respective forms

$$\rho_A U^2 S_A C_x = \rho v^2 S_H C_H \cos(\alpha+\beta), \tag{3.3a}$$

$$\rho_A U^2 S_A C_z = \rho v^2 S_H C_H \sin(\alpha+\beta) \tag{3.3b}$$

and

$$c_A C_M = C_z \Delta x - C_x \Delta z. \tag{3.3c}$$

The only parameters that may change with the angle of attack are C_x and C_z; C_M is independent of this angle by definition of the aerodynamic centre. Hence, the angle of attack at trim can be obtained as a solution of (3.3*c*). Given the angle of attack, the ratio of the first two equations,

$$\tan(\alpha+\beta) = (C_z/C_x), \tag{3.4}$$

yields the course relative to the wind; the sum of squares of these equations,

$$\rho_A S_A U^2 C_A = \rho S_H v^2 C_H = 2H, \tag{3.5}$$

where

$$C_A = \sqrt{C_z^2 + C_x^2}, \tag{3.6}$$

yields the speed.

3.2. Forces on the sail

The aerodynamic forces on the PMW sail can be categorized as shear forces, acting parallel to its surface, and pressure forces, acting perpendicular to it. The former contribute mainly to C_x; the latter dominate C_z and C_M, and contribute to C_x. It is shown in appendix C (see equations (C 25) and (C 29)) that for a sail with small aspect ratio,

$$C_z = C_{z,\alpha}\alpha + C_{z,\bar{f}}\bar{f} \tag{3.7}$$

and

$$C_M = -C_{M,\bar{f}}\bar{f}, \tag{3.8}$$

where $C_{z,\alpha}$, $C_{z,\bar{f}}$ and $C_{M,\bar{f}}$ are certain constants and $\bar{f}$ is the ratio of the sail camber to its chord. For the course of the following discussion, the exact values of these constants are immaterial—yet it is essential that all are positive and all are of unity magnitude. Since the camber of the PMW sail is small, a few per cent chord at most, the last term in (3.7) can usually be neglected. The experimental results of Torres & Mueller (2001) suggest that (3.7) holds up reasonably well to the angle of attack of 40°. We could not find experimental results to verify (3.8).

The contribution of the pressure loads to C_x is associated with the wing surface curvature. For a conventional wing section, this contribution is loosely divided into the contribution of the leading edge region and the contribution of the rest of the wing. The former is known as the leading edge suction, and it tends to decrease C_x as the angle of attack increases. The latter is commonly accounted for as a part of the 'parasite' drag, which includes the shear forces as well. It changes very little with the angle of attack as long as the flow pattern about the wing remains unchanged. For small aspect ratio wings, the leading edge suction is commonly neglected, leaving C_x practically independent of the angle of attack. The upper bound of C_x is estimated in appendix A to be approximately 0.1.

3.3. Trim control

Since C_z changes monotonically with the angle of attack, while C_x and C_M are independent of it, equation (3.3*c*) can be rewritten as

$$C_z = (c_A C_M + C_x \Delta z)/\Delta x. \tag{3.9}$$

It manifests that the side force and the angle of attack at trim are defined by the sail geometry (through C_M, which depends on the sail camber) and the relative location of the aerodynamic centre of the sail and the centre of effort of the hydrodynamic forces (through Δx and Δz).

On the right-hand side of (3.9), the denominator (Δx) is positive by stability considerations.[3] Hence, in order to obtain positive side force at trim (which is required to sail on the port tack), the numerator should be positive as well. In the numerator, C_x is positive (§3.2). Δz is positive by virtue of the inherent asymmetry of the PMW's float. At the same time, C_M is a decreasing function of the sail camber (see (3.8)). Hence, there is an upper bound, $(C_x \Delta z)/(c_A C_{M,\bar{f}})$, on the sail's camber.

The observations suggest that, with increasing wind speed (in particular, above 10 m s^{-1}), the angle of attack gradually vanishes (Totton & Mackie 1960, p. 322). Equation (3.9) provides three mechanisms that may explain this change in trim.

There can be a change in C_M; smaller C_M yields smaller C_z, and hence smaller angle of attack. The change in C_M is associated with the change in camber. It can come due to either (passive) aeroelastic deformation or (active) muscular contraction. There is probably no way to increase the camber passively with increasing wind speed. However, since the PMW is capable of changing its centre of buoyancy through muscular contraction (Totton & Mackie 1960, pp. 307, 374), it is plausible that the same mechanism can be used to change the camber actively.

There can be a change in C_x; smaller C_x yields smaller C_z. C_x decreases with the increasing wind speed owing to Reynolds number effects, but the associated change is estimated to be relatively small (appendix A).

There can be a change in the relative position between the aerodynamic centre of the sail and the

[3]Stability of a trimmed sail is manifested in maintaining its angle relative to the wind—a sudden increase in the angle of attack should produce a restoring couple. In other words, the derivative of the aerodynamic couple about HCE, $C_{M,H} = C_M + C_x \Delta z/c_A - C_z \Delta x/c_A$, with respect to the angle of attack should be negative. C_x, C_M, Δx and c_A are independent of the angle of attack, the first by assumption (§3.2), the others by definition; Δz slightly increases with the angle of attack through increasing roll (§4), whereas C_z increases monotonically with the angle of attack. Hence, for the derivative of $C_{M,H}$ to be negative, Δx should be positive.

centre of effort of the hydrodynamic forces. In particular, C_z at trim decreases as Δx increases or Δz decreases. The relative position of the two centres can change either due to list (roll) of the float or redistribution of the hydrodynamic drag. The former will be addressed in §4. Considering the latter, the drag is provided partly by large hunting tentacles and partly by other polyps. Drag coefficient of the large tentacles decreases with increasing sailing speed (figure 4). Drag coefficient of other polyps—which, presumably, remain as a block during sailing—should change very little as the sailing speed increases. Placing the longer tentacles aft causes the centre of effort to move forward as the sailing speed increases, increasing Δx; placing them at the maximal lateral distance to the side of the sail causes the centre of effort to move towards the sail, decreasing Δz.

In order to identify which of these mechanisms are relevant, consider a few representative figures. As mentioned already in §3.2, C_x is bounded from above by approximately 0.1. Judging from the available drawings (Totton & Mackie 1960, p. 310) the value of Δz can probably be bounded from above by $0.3c_A$. To make the numerator in (3.9) positive (see above), C_M should be greater than $-C_x\Delta z/c_A$, approximately -0.03. At the same time, judging from plate X in Totton & Mackie (1960), the camber is non-negative, and hence C_M is non-positive. Therefore, the numerator in (3.9) is bounded between 0 and approximately $0.03c_A$. But in order to obtain side-force coefficient of the order of unity, which is to be expected at the angle of attack of 40°, the denominator in (3.9) should be comparable with the numerator. Hence, Δx should be a few per cent of the sail chord. These figures imply that the trim of the PMW is a delicate one, and a minute shift of the centre of effort of the hydrodynamic forces or a minute change in the sail camber may change it completely.

Detailed description of the cormidia found in Totton & Mackie (1960, pp. 340–346) places the long tentacles aft and away from the sail. It implies that the passive trim control based on the tentacles' drag may be in use by the PMW. An indirect support to this conclusion is provided by the sailing speed of the PMW. In fact, the major part of the transition between the high and low angles of attack at trim should be completed when P of its hunting tentacles becomes of the order of 100 (figure 4). With $d=2$ mm, $C_{D,n}=1$ and $C_{D,t}=0.01$, P equals 100 at approximately $0.3\ \mathrm{m\ s^{-1}}$ when the tentacles have a negative buoyancy of 3 per cent, and approximately $0.4\ \mathrm{m\ s^{-1}}$ when they have a negative buoyancy of 5 per cent. These figures are comparable with the maximal sailing speed of approximately $0.4\ \mathrm{m\ s^{-1}}$ reported by Totton & Mackie (1960, p. 318).

Having the long tentacles positioned away from the sail and relatively aft infers that, when they capture prey, their effect on the trim is just the opposite of what has been previously discussed—an increase in their drag changes the trim towards higher angles of attack and hence amplifies the force on the tentacles. In order to prevent tearing the tentacles off and to allow pulling the prey towards the digesting polyps, the sail has to be 'sheeted out' (luffed). We believe that the PMW has the option to luff its sail by increasing the sail's camber through muscular contraction of the float. A change of the order of 1 per cent chord—a couple of millimetres—should suffice to this end (see equation (3.8) and the paragraph immediately following it).

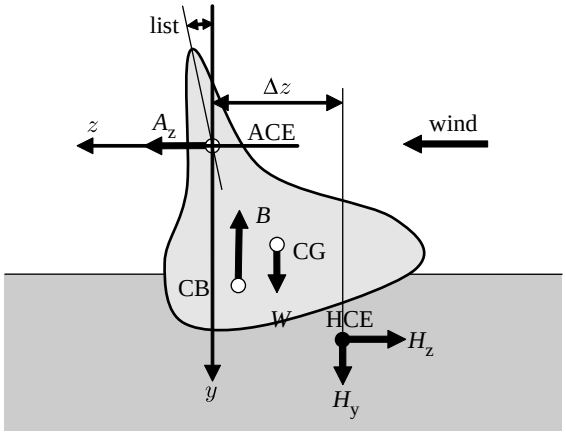

Figure 6. Schematic of the balance of forces when looking along the body. The sail generates the side force A_z, which is counterbalanced by sidewise hydrodynamic drag component H_z. The weight of the float W and the effective weight of all other polyps H_y are counterbalanced by the lift of the float B.

Passive speed control has no counterpart in the sailing world, where most autopilots are designed to keep the course, either relative to the wind or relative to the Earth, rather than to keep the speed relative to the water. Yet, presented with the requirement to keep the speed when drifting on a sea anchor, as in figure 2*b*, we can hardly think of a simpler design than that mimicking the PMW. Tie the sea anchor (representing here all the polyps other than the hunting tentacles) relatively forward on the port side, and hang a suitable non-buoyant long cable on the same side but astern. As the drift velocity increases, the cable will lift up, heading the boat into the wind and easing the sail.

4. LIST

As the angle of attack is a consequence of the balance of forces in the horizontal (x–z) plane, the roll angle (list) is a consequence of the balance of forces in the vertical (y–z) plane. A schematic balance of forces in the vertical plane is shown in figure 6. The horizontal side force on the sail, A_z, is counterbalanced by the respective component, H_z, of the hydrodynamic drag. The weight of the float, W, and the effective weight (weight minus lift) of all other polyps, H_y, are counterbalanced by the (mainly hydrostatic) lift of the float, B.

The point where the lift acts is marked 'CB' in figure 6. Listing to leeward moves this point to leeward as well. The list stabilizes when the couple produced by the lift counterbalances the couple produced by the aerodynamic forces on the sail–float and the hydrodynamic forces on all other polyps. Obviously, increasing A_z will increase the list to leeward; conversely, decreasing A_z will change the list to windward.

List to leeward increases Δz, and hence increases A_z by (3.9); in turn, increasing A_z increases the list. This is exactly what happens when a sudden gust hits. Until

the tentacles lift up and readjust the trim (it should take about the same time it takes the PMW to sail the length of its tentacles, approx. 30 s), the increasing force on the sail increases the list, which increases the angle of attack, which increases the list further (Totton & Mackie 1960, p. 322). This scenario reverses when the wind drops. A sudden lull decreases A_z, which changes the list to windward, which decreases A_z even further, possibly leading to a capsize (Totton & Mackie 1960, pp. 309, 374). A consequence of this amplification of the list is the existence of minimal wind strength allowing the PMW to use its sail.

Capsizing appears as a single obstacle that prevents the PMW from changing tacks (Totton & Mackie 1960, p. 321). In fact, by increasing the camber of the sail, the numerator in (3.9) can be made negative, resulting in negative A_z. Negative A_z implies sailing on a starboard tack.

5. COURSE AND SPEED

The course of the PMW relative to the wind is determined solely by the angle of attack at trim. From (3.4)

$$\beta = \tan^{-1}(C_z/C_x) - \alpha. \tag{5.1}$$

The largest angle from downwind, β^*, is obtained at the angle of attack α^*, which is the solution of $\mathrm{d}\beta/\mathrm{d}\alpha = 0$. Since C_x was assumed already to be independent of α, differentiating the right-hand side of (5.1) with respect to α yields

$$\frac{C_x}{C_x^2 + C_z^2}\frac{\mathrm{d}C_z}{\mathrm{d}\alpha} - 1 = 0. \tag{5.2}$$

With C_z given by (3.7), the solution of (5.2) is

$$C_z^* = \sqrt{C_{z,\alpha}C_x - C_x^2}, \tag{5.3}$$

at which

$$\beta^* = \tan^{-1}\left(\frac{\sqrt{C_{z,\alpha}C_x - C_x^2}}{C_x}\right) - \frac{\sqrt{C_{z,\alpha}C_x - C_x^2}}{C_{z,\alpha}} + \frac{C_{z,\bar{f}}\bar{f}}{C_{z,\alpha}}. \tag{5.4}$$

Consider typical figures. As already mentioned above, C_x is of the order of 0.1; $C_{z,\alpha}$ and $C_{z,\bar{f}}$ are about unity; $\bar{f}$ is a few hundredths, and hence insignificant. Thus, C_z^* is approximately 0.3, corresponding to α^* of 15–20° and β^* of 50–55°. In comparison, at the angle of attack of 40°, equation (5.1) yields β of 40–45°, about the value reported by Totton & Mackie (1960, p. 321). This means that, by reducing the angle of attack, the PMW could have achieved a better course relative to the wind. It is therefore plausible that the course relative to the wind was not the aim of the PMW's design. Rather, its design was probably aimed at keeping the pull of the sail as constant as possible (independent of the wind speed) so as to allow the best possible conditions for the tentacles to spread out.

In order to estimate the sailing speed, data are required concerning the hydrodynamic drag H. It includes the drag of long (hunting) tentacles, H_t, and the combined drag of all other polyps, H_p. For simplicity, the drag of the last group will be approximated with a simple constitutive relation

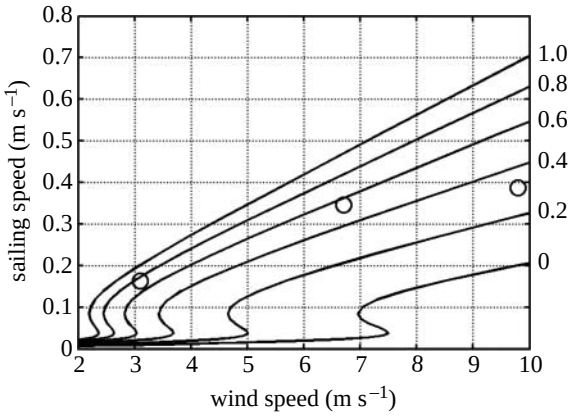

Figure 7. Sailing speed as a function of wind speed at constant side-force coefficient C_z, the value of which is marked to the right of each line. The circles are based on the observations cited in Totton & Mackie (1960).

$$H_\mathrm{p} = \frac{1}{2}\rho S_\mathrm{p} v^2 C_{\mathrm{H,p}} = F_\mathrm{g} P \frac{S_\mathrm{p} C_{\mathrm{H,p}}}{dlC_{\mathrm{D,n}}}, \tag{5.5}$$

where S_p is a suitable reference area; $C_{\mathrm{H,p}}$ is the associated drag coefficient; and all remaining quantities pertain to the average tentacle. The drag of N tentacles will be approximated as N times the drag of the average tentacle, i.e.

$$H_\mathrm{t} \approx NF_\mathrm{g}\left(P\frac{C_{\mathrm{D,t}}}{C_{\mathrm{D,n}}}\left(\frac{-1+\sqrt{1+4P^2}}{2P}\right)^3 + \frac{1}{\sqrt{P}}\left(\frac{-1+\sqrt{1+4P^2}}{2P}\right)^{3/2}\right), \tag{5.6}$$

see (2.10), (2.4) and (2.11). With (5.5) and (5.6), equation (3.5) for the sailing speed can be recast as an algebraic equation for P,

$$\frac{\rho_\mathrm{A} S_\mathrm{A} U^2 C_\mathrm{A}}{2NF_\mathrm{g}} = P\frac{C_{\mathrm{D,t}}}{C_{\mathrm{D,n}}}\left(\frac{-1+\sqrt{1+4P^2}}{2P}\right)^3 + \frac{1}{\sqrt{P}}\left(\frac{-1+\sqrt{1+4P^2}}{2P}\right)^{3/2} + P\frac{S_\mathrm{p} C_{\mathrm{H,p}}}{NdlC_{\mathrm{D,n}}}. \tag{5.7}$$

We assume that a representative (nominal) PMW (appendix A) has sail area S_A of 0.01 m^2 and seven tentacles; the average tentacle is 10 m long, 2 mm in diameter, has a negative buoyancy of 3 per cent and is characterized by $C_{\mathrm{D,n}} = 1$ and $C_{\mathrm{D,t}} = 0.01$. These set its weight in the water, F_g, at approximately 1 g. The drag area of its digesting and reproductive polyps, $S_\mathrm{p}C_{\mathrm{H,p}}$, is guessed as 0.001 m^2. With these, the solution of (5.7) is shown in figure 7. At each value of C_z, the sharp increase in the sailing speed corresponds to the lifting of the tentacles towards the horizontal—these are exactly the conditions where the spreading of the tentacles is the most effective. The observations of the sailing

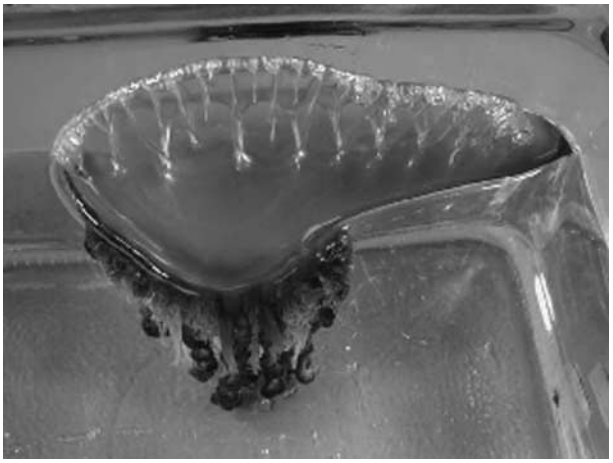

Figure 8. Top view of the PMW. The picture is courtesy of the Southeastern Regional Taxonomic Center at the South Carolina Department of Natural Resources.

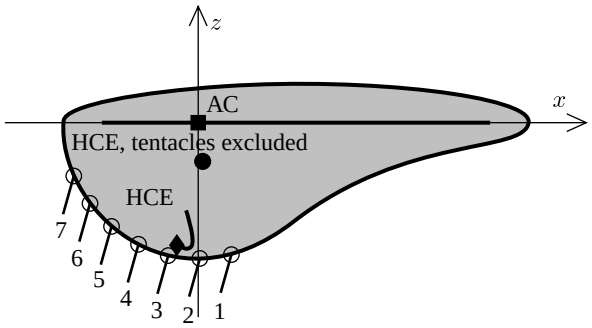

Figure 9. Top view of the nominal PMW. There are seven long tentacles, differing in length and diameter. The lengths are uniformly distributed between 15 and 5 m; tentacle 1 being the longest and tentacle 7 being the shortest. The diameters are uniformly distributed between 3 and 1 mm, tentacle 1 being the thickest and tentacle 7 the thinnest. The HCE changes with sailing speed; its low-speed value is marked by a diamond.

speed reported by Totton & Mackie (1960) are marked by the circles.[4] They inferred that C_z decreases as the wind speed increases (i.e. the PMW 'sheets out' its sail), and that the stronger winds are hardly optimal for spreading the tentacles.

6. AN EXAMPLE

To elucidate the trim of the sail, consider now a more elaborate model of the PMW. This artificial model is entirely made up to serve as an illustrating example. In this model, we guess the centre of effort of the hydrodynamic forces acting on the block of digesting and reproductive polyps, differentiate the seven long tentacles by length and diameter, and specify their connection points with the float. The geometry (mimicking the PMW depicted in figure 8) is shown in figure 9; the associated numbers can be found in appendix A.

To simplify the solution of (3.5) we invert the approach of §5 and assume the sailing speed, v, rather than the wind speed, U, to be the independent variable. Given v, P for each tentacle immediately follows from (2.4). The tilt angles of the tentacles follow from (2.3); the associated drag forces follow from (2.10); the drag of all other polyps follows from (5.5). The knowledge of the drag forces allows the HCE to be found; the trim follows from (3.3c). Once the trim is known, the wind speed and the course relative to the wind follow from (3.5) and (3.4). The results of this procedure are shown in figure 10, once for $C_M = -0.01$ (solid curves) and once for $C_M = -0.023$ (dashed curves).

The 'L'-shaped track of the HCE in figure 9 is an immediate consequence of our placing the thin (and hence the fastest to lift up) tentacles forward and close to the sail. As the speed increases and the thin tentacles begin lifting, the centre of effort moves aft; once the bigger tentacles (located to the side of the sail) begin lifting, it moves inward. We remind readers that this is just an example and this track could have been shaped at will by altering the diameters and the lengths of the tentacles, their connection points, etc.

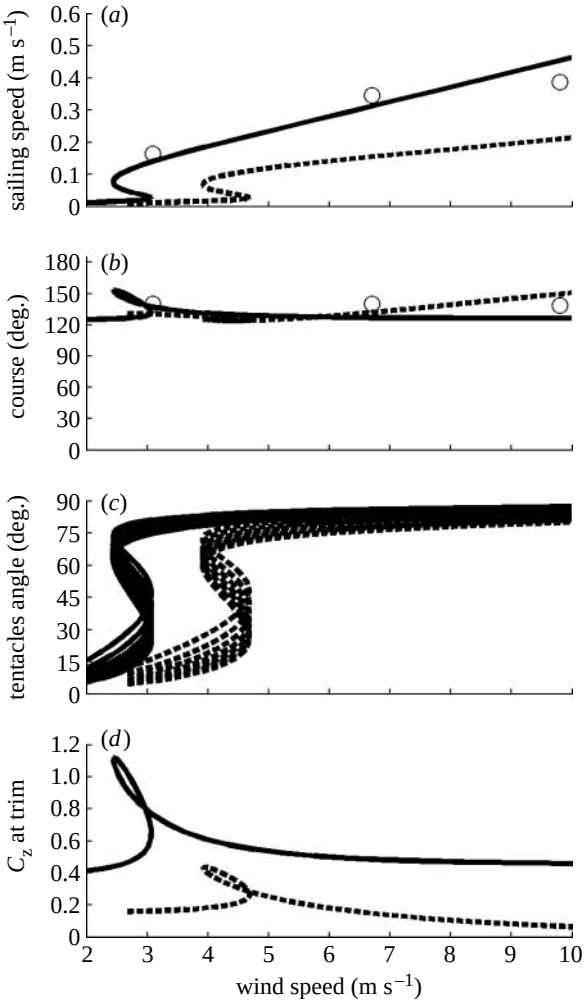

Figure 10. (a–d) Performance of the nominal PMW with $C_M = -0.01$ (solid curves) and $C_M = -0.023$ (dashed curves). The observations reported in Totton & Mackie (1960) are marked by circles. The multitude of curves in (c) mark individual tentacles, the lowest corresponding to tentacle 1. The course in (b) is measured relative to the wind.

[4] The two higher speed observations are reported in full on their p. 319. The lower speed observation, appearing on their p. 322, lacks the actual sailing speed. We estimated it from the course direction (40° from downwind) and from the normal to the wind velocity component of 0.13 m s^{-1} (1/4 knot).

The angular spread of the tentacles is biggest in light winds (figure 10*c*). The wind speed at which this best spreading occurs is influenced by many parameters of the model, conspicuously by C_M, but also by the negative buoyancy of the tentacles and their diameters. C_M controls the angle of attack; the buoyancy and the diameters control the sailing speed at which the tentacles lift up (through P).

The sailing speed rapidly increases in light winds, from practically 0 at 2 m s^{-1} to more than 0.1 m s^{-1} at 2.5 m s^{-1} (with $C_M = -0.01$). This behaviour was reported by Totton & Mackie (1960, p. 322); it is an immediate consequence of the tentacles losing drag as they lift towards horizontal (§2). A minute decrease in C_M, from -0.01 to -0.023, corresponding to an increase of less than 1 per cent chord in camber, is sufficient to luff the sail almost completely—compare solid and dashed curves in figure 10*d*.

7. CONCLUDING REMARKS

The most conspicuous results of this study can be summarized in three points as follows.

(i) The tilt angle (from vertical) of a trailing tentacle increases with the sailing velocity and decreases with the tentacle diameter. Since the tentacles are of different diameters, trailing causes them to spread fan-like in the vertical plane. The spread angle vanishes both at small and at large trailing speeds. Using plausible figures for the diameters, densities and drag coefficients of the tentacles, the spread angle is estimated as 10–15° at the same speeds the PMW were observed sailing.

(ii) The force needed to trail a tentacle at a given speed decreases as the tilt angle of the tentacle increases. The tentacles bud from the float in such a way that this change in drag sheets out the sail as the tentacles lift up, which serves to keep the sailing speed in that particular range where the tentacles spread best. The PMW were observed sailing with their sails aligned with the wind in strong winds.

(iii) The trim of the sail is very delicate and a minute increase in camber may luff the sail.

We believe that these results can be rationalized by adopting a hypothesis that the PMW has evolved for efficient sail-driven trawling: the tentacles' spreading obviously increases the likelihood of catching the prey (Madin 1988; Purcell 1997), whereas the PMW 'does' all it possibly can to keep them spread.

We hope that this study will encourage new observations and measurements that will allow for a better understanding of this singular colony. A partial list of missing data includes tentacles' dimensions, density and attachment points to the float, float geometry and drag of all polyps which are not the hunting tentacles.

APPENDIX A. THE NOMINAL PMW

A.1. Models

To rationalize the analysis, we define a representative ('nominal') PMW. There are many parameters characterizing a PMW, ranging from its sail area, to the connection point of the largest tentacle in a specific cormidium. Unfortunately, many of these parameters have never been measured. As a result, they had to be guessed based on our best experience, or deduced indirectly from other data. The parameters that were guessed are underlined below. Examples of §§2–4 are based on the relatively well-established data; the example of §6 involves a considerable guesswork.

A.2. Air and water data

All examples in the text are based on the standard air density of 1.225 kg m^{-3} and seawater density of 1030 kg m^{-3}.

A.3. The sail

Above the water level, the PMW consists of a smooth float with a corrugated crest (figures 1 and 8). The edge of the crest makes this combination work as a single sail by promoting flow separation when set at an angle to the wind.[5]

We assume that the projection of the sail (the crest and the part of the float above the water) on the plane $z=0$ (figure 5) has the area S_A of 100 cm^2, average chord c_A of 25 cm and height h of 6 cm; the crest has the surface area S_c of 100 cm^2, surface roughness to length ratio of 1/100 and edge thickness of 7 mm; the float has the surface area S_f of 100 cm^2 and slenderness ratio of 3 (Raymer 1992, pp. 280–281).

Based on these data, C_x was estimated using the component build-up method (Raymer 1992, pp. 279–281), i.e.

$$C_x = (S_f/S_A)C_{x,f} + (S_c/S_A)C_{x,c}, \qquad (A\,1)$$

where $C_{x,f}$ and $C_{x,c}$ are the respective drag coefficients. Assuming a laminar boundary layer on the float, $C_{x,f}$ varies[6] between approximately 0.03 and approximately 0.01 as the Reynolds numbers (based on the float length) increase from 2×10^4 to 2×10^5; assuming a turbulent boundary layer the respective range of $C_{x,f}$ is between approximately 0.03 and approximately 0.02. For a 25 cm float, the Reynolds numbers between 2×10^4 and 2×10^5 correspond to wind speeds between 1.2 and 12 m s^{-1}. Assuming a turbulent boundary layer, and a stagnant wake having about the same thickness t and width h as the crest's edge, $C_{x,c}$ turns out to be approximately 0.06, independent of the Reynolds number.[7] The contribution of the wake, th/S_c, is responsible for approximately two-thirds of $C_{x,c}$. These estimates yield C_x between approximately 0.07

[5]Just as any winged slender body configuration (Ashley & Landahl 1985, p. 122).
[6]Pertinent equations in Raymer (1992) are (12.24), (12.25), (12.27) and (12.31).
[7]Pertinent equations in Raymer (1992) are (12.27) as (12.28).

and approximately 0.09 by (A 1). Considering possible inaccuracy of this estimate, all examples in the text are based on $C_x = 0.1$.

The side-force coefficient C_z was estimated with equation (C 23)[8] of appendix C using the aspect ratio[9] A of 0.7. C_z turns out to be approximately 0.8 at the angle of attack of 40°. The moment coefficient about the aerodynamic centre, C_M, was estimated with equation (C 29).[10] With 1 per cent camber, C_M is approximately -0.02.

A.4. Submerged body parts which are not tentacles

This group includes all polyps which are not the hunting tentacles and the float. The drag area of this group (reference area times the drag coefficient) was estimated, based on the pictures in Totton & Mackie (1960, plate IX), as 10 cm^2. The respective centre of effort was placed at 1 per cent chord aft of the aerodynamic centre of the sail (along the x-axis) and 10 per cent chord to windward (along the negative z-axis; figure 9). The last parameter was guessed from drawings in Totton & Mackie (1960, pp. 340–341); the first was adjusted in the range of 5 per cent chord aft to 5 per cent chord forward of the aerodynamic centre so as to obtain meaningful results.

A.5. Tentacles

Following Totton & Mackie (1960, pp. 340–341), seven long tentacles were assumed, one in each cormidium. The average tentacle was assumed to be cylindrical, 10 m long and 2 mm in diameter. No reference could be found for the density of a tentacle. Based on fishes (Davenport 2005), it was assumed that the tentacles have 3 per cent negative buoyancy, but this estimate obviously needs verification.

The drag coefficient of a circular cylinder in cross-flow varies between approximately 1.4 and approximately 1 as the cross-flow Reynolds numbers (based on the diameter and the cross-flow velocity) vary between 10^2 and 10^3 (Batchelor 1990, p. 341). For a 2 mm cylinder in the water, this range corresponds to the cross-flow velocities between 0.05 and 0.5 m s^{-1}. At slower speeds, the drag coefficient dramatically increases; at higher speeds it remains practically constant (Batchelor 1990, p. 341). In the examples, we took $C_{D,n} = 1$ for all tentacles.

The drag coefficient of a circular cylinder in axial flow varies between approximately 0.005π and approximately 0.003π as the axial flow Reynolds number (based on the length and axial flow velocity) varies between 10^6 and 10^7. This estimate is based on eqn (12.27) in Raymer (1992, p. 280) under the assumption of turbulent boundary layer; in this range of Reynolds numbers, maintaining the laminar boundary layer is hardly possible. For a 10 m long cylinder in the water, Reynolds numbers between 10^6 and 10^7 correspond to the axial velocities between 0.1 and 1 m s^{-1}. In the examples, we took $C_{D,t} = 0.01$ to represent the upper range of sailing speeds.

For the example in §6, the seven individual tentacles were differentiated. Their lengths were uniformly distributed between 15 and 5 m, the tentacle of cormidium 1 being the longest. Likewise, their diameters were uniformly distributed between 1 and 3 mm; again, the tentacle of cormidium 1 being the thickest (figure 9). The connection points were chosen on a circle, centred at the aerodynamic centre of the sail; the respective coordinates (x, z), by cormidium order, being $(8, -34)$, $(0, -35)$, $(-8, -34)$, $(-16, -31)$, $(-22, -27)$, $(-28, -21)$ and $(-32, -14)$ per cent chord relative to the aerodynamic centre of the sail (figures 8 and 9).

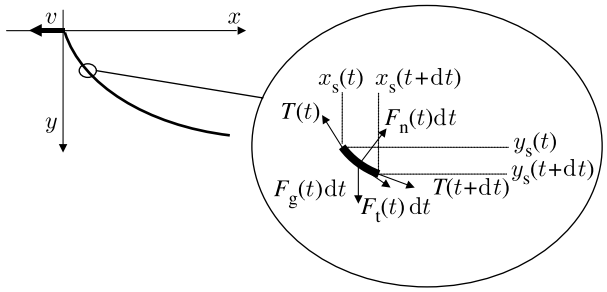

Figure 11. The tentacle and the balance of forces on its element.

APPENDIX B. THE SHAPE OF A TRAILING TENTACLE

B.1. Formulation

Consider a tentacle of length l and uniform diameter d being pulled horizontally through the water by its end. Let ρ_t and ρ be the densities of the tentacle and the water, g the acceleration of gravity and v the (constant) trailing velocity. The following analysis will be assisted by the use of dimensionless quantities, with l serving as the reference length and $\pi(\rho_t - \rho)d^2 g/4$ serving as the reference force per unit length.

We shall adopt a Cartesian coordinate system with the y-axis pointing along the direction of gravity, the x-axis opposing the velocity vector, and the origin fixed at the end of the tentacle by which it is pulled (figure 11).

The shape of the tentacle is assumed to be defined by the pair of monotonically increasing functions on the interval [0,1], x_s and y_s, such that

$$x = x_s(t), \qquad y = y_s(t), \tag{B 1}$$

where t is the (dimensionless) distance to the origin along the tentacle. Accordingly, with prime standing for a derivative,

$$x_s'^2 + y_s'^2 = 1, \tag{B 2}$$

on (0,1), and

$$x_s(0) = y_s(0) = 0. \tag{B 3}$$

When trailing, the tentacle is affected by the hydrodynamic and gravity forces. The latter (per unit length of the tentacle) is simply

$$F_g = 1, \tag{B 4}$$

[8]In notation of appendix C, $C_z = 2F_z/(\rho S v_2)$.
[9]For a sail, protruding perpendicular to an impermeable water surface, aspect ratio is defined as twice the height of the sail squared divided by its area (appendix C).
[10]In notation of appendix C, $C_M = 2M/(\rho S c v_2)$.

it acts along the y-axis. The hydrodynamic force (per unit length) consists of tangential (axial) F_t and normal F_n components, assumed to obey the constitutive relations

$$F_t = pC_t, \qquad F_n = pC_n, \tag{B 5}$$

where

$$p = \frac{\rho}{\rho_t - \rho}\frac{2v^2}{\pi g d} \tag{B 6}$$

is a convenient dimensionless parameter, and C_t and C_n are the respective hydrodynamic coefficients. Both are positive, and, in general, are functionals of x_s and y_s. In what follows, it will be assumed that they depend on the local values of x_s' or y_s' only.

It is postulated that the tension T in the tentacle is a monotonic non-negative function on [0,1], vanishing at the free end, i.e.

$$T(1) = 0. \tag{B 7}$$

T satisfies the pair of equilibrium conditions on (0,1),

$$\left(Tx_s'\right)' + p\left(C_t x_s' + C_n y_s'\right) = 0 \tag{B 8a}$$

and

$$\left(Ty_s'\right)' + p\left(C_t y_s' - C_n x_s'\right) + 1 = 0, \tag{B 8b}$$

representing the y- and x-components of the force balance on an infinitesimally small element of the cable (figure 11). We seek the solution of these equations satisfying (B 2), (B 3) and (B 7).

B.2. General solution

A straightforward solution of equations (B 8a) and (B 8b) for T and T' yields

$$T = \frac{pC_n}{D}\left(x_s'^2 + y_s'^2\right) - \frac{1}{D}x_s'^2 \tag{B 9a}$$

and

$$T_s' = -pC_t + \frac{pC_n}{D}\left(x_s'' x_s' + y_s'' y_s'\right) + \frac{1}{D}x_s'', \tag{B 9b}$$

where

$$D = y_s'' x_s' - x_s'' y_s'. \tag{B 10}$$

The sum in the parenthesis on the right-hand side of (B 9a) equals unity by (B 2); moreover,

$$x_s'' x_s' + y_s'' y_s' = \frac{1}{2}\left(x_s'^2 + y_s'^2\right)' = 0, \tag{B 11}$$

by (B 2) as well, and hence

$$D = y_s''/x_s' = -x_s''/y_s'. \tag{B 12}$$

Consequently, equations (B 9a) and (B 9b) can be recast into the respective forms

$$Ty_s'' = x_s'\left(pC_n - x_s'\right) \tag{B 13a}$$

and

$$T' = -pC_t - y_s'. \tag{B 13b}$$

Since the tension vanishes at the free end,

$$x_s' = pC_n \tag{B 14}$$

at $t=1$, by (B 7) and (B 13a). With C_n being a known (but still unspecified) function of x_s'—see the paragraph immediately following (B 6)—equation (B 14) can be solved, at least in principle, to obtain $x_s'(1)$. This value will be denoted as 'a'; i.e. $x_s'(1) = a$ satisfies (B 14).

Picking the clue from (B 14), we suggest that

$$x_s' = x_s'(1) = a \tag{B 15}$$

on the entire interval (0,1) is a valid solution of (B 13a) and (B 13b). In fact, in this case, the product Ty_s'' vanishes on (0,1) by (B 13a) and (B 14). But constant x_s' on [0,1] implies constant

$$y_s' = \sqrt{1 - x_s'^2} = \sqrt{1 - a^2}, \tag{B 16}$$

on (0,1) by (B 2), which, in turn, implies $y_s'' = 0$. Thus, (B 13a) is identically satisfied if the tentacle takes on the shape of a straight line at an angle with the vertical. This conclusion agrees with the known results (Hoerner 1965, p. 13.20).

This solution can be complemented by integrating (B 13b) for the tension. With constant y_s', it is a linearly decreasing function

$$T(t) = T(0)(1 - t), \tag{B 17}$$

along the tentacle, where

$$T(0) = pC_t + y_s' = pC_t + \sqrt{1 - x_s'^2} \tag{B 18}$$

is the tension at the end by which the tentacle is pulled.

B.3. Particular solution

Now, consider a particular case when the hydrodynamic coefficients are given by

$$C_n = C_{D,n} y_s'^2 = C_{D,n}\left(1 - x_s'^2\right) \tag{B 19a}$$

and

$$C_t = C_{D,t} x_s'^2 = C_{D,t}\left(1 - y_s'^2\right), \tag{B 19b}$$

where $C_{D,n}$ and $C_{D,t}$ can be interpreted as drag coefficients of the tentacle in cross-flow and axial flow, respectively. At the pertinent flow regimes (characterized by the Reynolds number), $C_{D,n}$ is of the order of unity, whereas $C_{D,t}$ is two orders of magnitude smaller (appendix A). The variants on the right-hand side of (B 19a) and (B 19b) follow those preceding them by (B 2).

With (B 19a), the conjunction of (B 14) and (B 15) takes on the form

$$x_s' = pC_{D,n}\left(1 - x_s'^2\right), \tag{B 20}$$

with the obvious solution

$$x_s' = a = \frac{-1 + \sqrt{1 + \left(2pC_{D,n}\right)^2}}{2pC_{D,n}}; \tag{B 21}$$

the sign in the numerator is chosen so as to obtain $x_s' \geq 0$.

The conjunction of (B 18), (B 20) and (B 21) yields the tension

$$T(0) = pC_{\mathrm{D,t}}x_{\mathrm{s}}'^2 + \sqrt{\frac{x_{\mathrm{s}}'}{pC_{\mathrm{D,n}}}}, \qquad \text{(B 22)}$$

and, in turn, the horizontal,

$$F_X = T(0)x_{\mathrm{s}}' \qquad \text{(B 23)}$$

and vertical,

$$F_Y = T(0)y_{\mathrm{s}}', \qquad \text{(B 24)}$$

components of the force acting on the entire tentacle.

B.4. Uniqueness

A note on the uniqueness of the proposed solution is in order. To this end, introduce (B 19*a*) in (B 13*a*); this yields

$$Ty_{\mathrm{s}}'' = x_{\mathrm{s}}'\left(pC_{\mathrm{D,n}} - pC_{\mathrm{D,n}}x_{\mathrm{s}}'^2 - x_{\mathrm{s}}'\right). \qquad \text{(B 25)}$$

Note that $x_{\mathrm{s}}' = a$ is the largest positive root of the right-hand side. Hence, the right-hand side of (B 25) turns negative if $x_{\mathrm{s}}' > a$, and positive if $x_{\mathrm{s}}' < a$. Assume, for the sake of argument, that $x_{\mathrm{s}}' > a$. Since the tension cannot be negative, the negative right-hand side of (B 25) implies $y_{\mathrm{s}}'' < 0$. With (B 11), this implies $x_{\mathrm{s}}'' > 0$, i.e. a monotonically increasing x_{s}' along the tentacle. But x_{s}' should equal a at $t=1$ by (B 14); hence a monotonically increasing x_{s}' implies that x_{s}' should be smaller than a for the entire tentacle length, which contradicts the initial assumption. The same arguments rule out $x_{\mathrm{s}}' < a$.

APPENDIX C. SLENDER SAIL THEORY

The flow field about a sail is obviously affected by the presence of the water surface. Given the characteristic dimensions of the PMW's sail, this surface can be approximated, with very good accuracy, as planar. A common technique of finding the flow field in a half-space bounded by an impermeable planar surface is by extending the flow field over the entire space and imposing symmetry with respect to the plane that previously was the boundary (Milne-Thomson 1996, pp. 219–220). Thus, the flow field about the sail protruding above the water surface is approximately the same as the flow field about a symmetric wing, comprising the sail and its mirror image, in an unbounded domain.

The PMW sail is slender and has a substantial thickness. Yet, as long as it has a distinct trailing edge, the aerodynamic forces acting on it will be comparable (of the same magnitude) with those acting on an infinitely thin slender wing having the same planform. This statement can be rigorously proved, but the proof is too long for the scope of this appendix. An indirect proof is in the well-known equality between the lift of a thin delta wing and a lift of a cone, having the same diameter as the span of the wing (Ashley & Landahl 1985, pp. 122–123). Since the derivations involving a thick winged body are incomparably more complicated than those involving just a wing, the following derivations will address the latter. They will loosely follow the procedure outlined in Bisplinghoff *et al.* (1996, pp. 244–248).

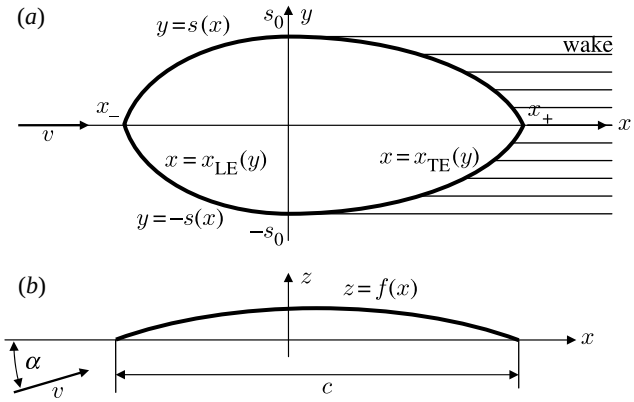

Figure 12. Wing geometry. (*a*) Top view and (*b*) side view.

Consider a thin slender wing with swept forward trailing edge and left–right symmetry moving in an unbounded domain of fluid (figure 12). A convenient right-handed Cartesian coordinate system will have its x-axis pointing backward (roughly, downwind) and passing through the foremost and aftermost points of the wing, y-axis pointing to the right and passing through the leftmost and rightmost points of the wing, and z-axis pointing upward. Thus, the leading edge of the wing is the edge of the wing lying forward of the plane $x=0$; the trailing edge is the edge of the wing lying aft of the same plane. The coordinates of the foremost, aftermost, leftmost and rightmost points on the wing are $(x_-, 0, 0)$, $(x_+, 0, 0)$, $(0, -s_0, 0)$ and $(0, s_0, 0)$, respectively (figure 12).

The outline of the wing's projection onto the plane $z=0$ can be defined either by specifying its left and right edges,

$$y = -s(x) \quad \text{and} \quad y = s(x), \qquad \text{(C 1)}$$

or by specifying its leading and trailing edges,

$$x = x_{\mathrm{LE}}(y) \quad \text{and} \quad x = x_{\mathrm{TE}}(y), \qquad \text{(C 2)}$$

respectively. $s : [x_-, x_+] \to [0, s_0]$ is assumed to be continuous on $[x_-,0]$, non-decreasing on $[x_-,0)$, piecewise continuous and non-increasing on $(0,x_+]$ and vanishing at its edges: $s(x_-) = s(x_+) = 0$; obviously, $s(0) = s_0$. $x_{\mathrm{LE}} : [-s_0, s_0] \to [x_-, 0]$ and $x_{\mathrm{TE}} : (-s_0, s_0) \to (0, x_+]$ are assumed continuous and even, with $x_{\mathrm{LE}}(\pm s_0) = x_{\mathrm{TE}}(\pm s_0) = 0$, $x_{\mathrm{LE}}(0) = x_-$ and $x_{\mathrm{TE}}(0) = x_+$. The chord c of the wing is, by definition, the distance between its foremost and aftermost points, and hence $c = x_+ - x_-$. The span b of the wing is, by definition, the distance between its leftmost and rightmost points, and hence $b = 2s_0$. The wing area S is commonly defined as the area of the wing's projection onto the plane $z=0$; it can be computed using either (C 1) or (C 2):

$$S = \int_{-s_0}^{s_0} (x_{\mathrm{TE}}(y) - x_{\mathrm{LE}}(y))\mathrm{d}y = 2\int_{x_-}^{x_+} s(x)\mathrm{d}x. \qquad \text{(C 3)}$$

Finally, the aspect ratio of the wing A is defined as $A = b^2/S$. It will be assumed that A is small when compared with unity.

The wing surface will be assumed smooth with no span-wise curvature; it will be defined by

$$z = f(x), \tag{C 4}$$

where f is a function on $[x_-,x_+]$. It will be assumed that the first derivative of f is piecewise continuous and small when compared with unity on (x_-,x_+), and $f(x_-)=f(x_+)=0$; these imply that f is small when compared with the wing's chord.

Now, let this wing move symmetrically at the angle of attack α with constant velocity v in an unbounded domain of quiescent fluid of density ρ (figure 12); α will be assumed small when compared with unity. The fluid will be assumed inviscid and irrotational everywhere, except for an infinitesimally thin vortical wake, postulated to extend from the trailing edge to infinity. Confining the solution to the leading order with respect to the angle of attack, it can be assumed that the wake is rectilinear and coplanar with the wing for any x in $(0,x_+]$.

Let p and μ be the pressure and potential jumps across the wing or wake surfaces. Under the assumption that the angle of attack is small, the two are related by

$$p = -\rho v \partial\mu/\partial x \tag{C 5}$$

(Bisplinghoff *et al.* 1996, pp. 246). Since there can be no pressure discontinuity across the wake, (C 5) implies

$$\partial\mu/\partial x = 0 \tag{C 6}$$

on the wake. The z-component of the aerodynamic force acting on the wing, F_z, and the couple about the y-axis, M, immediately follow (C 5) by simple quadratures

$$F_z = \rho v \int_{-s_0}^{s_0} \mathrm{d}y \int_{x_{\mathrm{LE}}(y)}^{x_{\mathrm{TE}}(y)} \frac{\partial\mu(x,\,y)}{\partial x}\,\mathrm{d}x \tag{C 7a}$$

$$= \rho v \int_{x_-}^{x_+} \mathrm{d}x \int_{s(x)}^{s(x)} \frac{\partial\mu(x,\,y)}{\partial x}\,\mathrm{d}y, \tag{C 7b}$$

and

$$M = -\rho v \int_{-s_0}^{s_0} \mathrm{d}y \int_{x_{\mathrm{LE}}(y)}^{x_{\mathrm{TE}}(y)} \frac{\partial\mu(x,\,y)}{\partial x}\,x\,\mathrm{d}x \tag{C 8a}$$

$$= -\rho v \int_{x_-}^{x_+} x\,\mathrm{d}x \int_{s(x)}^{s(x)} \frac{\partial\mu(x,\,y)}{\partial x}\,\mathrm{d}y, \tag{C 8b}$$

both the equations are correct in the leading order with respect to the wing's camber only.

Under the assumption that the aspect ratio of the wing is small when compared with unity, the problem of finding the potential jump across the wing's surface can be eventually reduced to the solution of the integral equations (Bisplinghoff *et al.* 1996, pp. 245),

$$\frac{1}{2\pi} \int_{-s(x)}^{s(x)} \frac{\partial\mu(x,\zeta)}{\partial\zeta} \frac{\mathrm{d}\zeta}{y-\zeta} = v_\perp(x), \tag{C 9}$$

for each x in $(x_-,0]$ and y in $(-s(x),\,s(x))$ and

$$\frac{1}{2\pi} \int_{-s(0)}^{s(0)} \frac{\partial\mu(x,\zeta)}{\partial\zeta} \frac{\mathrm{d}\zeta}{y-\zeta} = v_\perp(x), \tag{C 10}$$

for each x in $(0,x_+)$ and y in $(-s(x),\,s(x))$.

The quantity

$$v_\perp(x) = v\left(\alpha - \frac{\mathrm{d}f(x)}{\mathrm{d}x}\right) \tag{C 11}$$

on the right-hand side of (C 9) and (C 10) is the velocity component normal to the wing surface. The bar across the integral sign indicates the Cauchy principal value.

The solution of (C 9),

$$\frac{\partial\mu(x,\,y)}{\partial y} = -\frac{2v_\perp(x)}{\pi\sqrt{s^2(x)-y^2}} \fint_{s(x)}^{-s(x)} \frac{\sqrt{s^2(x)-\zeta^2}}{y-\zeta}\,\mathrm{d}\zeta$$

$$= -\frac{2v_\perp(x)y}{\sqrt{s^2(x)-y^2}}, \tag{C 12}$$

immediately follows by Sohngen inversion (Ashley & Landahl 1985, pp. 91–93; Bisplinghoff *et al.* 1996, pp. 217, 246). Since there can be no potential jump ahead of (and hence at) the leading edge (Bisplinghoff *et al.* 1996, p. 245), integration of (C 12) readily yields

$$\mu(x,\,y) = 2v_\perp(x)\sqrt{s^2(x)-y^2}, \tag{C 13}$$

for any x in $(x_-,0]$ and y in $(-s(x),\,s(x))$.

Returning to (C 10), we note that, in the integral on the left-hand side, the region where ζ is in the exterior of $(-s(x),\,s(x))$ belongs to the wake. On that region, $\partial\mu/\partial x$ vanishes by (C 6), and hence

$$\partial^2\mu(x,\zeta)/\partial x\,\partial\zeta = 0, \tag{C 14}$$

for any x in $(0,x_+)$ and ζ not in $(-s(x),\,s(x))$, by (C 6). Thus, differentiating (C 10) with respect to x, one readily obtains

$$\frac{1}{2\pi} \int_{-s(x)}^{s(x)} \frac{\partial^2\mu(x,\zeta)}{\partial x\,\partial\zeta} \frac{\mathrm{d}\zeta}{y-\zeta} = \frac{\mathrm{d}v_\perp(x)}{\mathrm{d}x}, \tag{C 15}$$

for each x in $(0,x_+)$ and y in $(-s(x),\,s(x))$. Its solution, by analogy with (C 9) and (C 13), is

$$\frac{\partial\mu(x,\,y)}{\partial x} = 2\frac{\mathrm{d}v_\perp(x)}{\mathrm{d}x}\sqrt{s^2(x)-y^2}, \tag{C 16}$$

for any x in $(x_-,0]$ and y in $(-s(x),\,s(x))$. Unfortunately, this equation cannot be integrated in the general case to obtain μ, but once the span and the camber have been specified, μ should follow.

The integral forces acting on the wing are given by (C 7*a*) or (C 7*b*) and (C 8*a*) or (C 8*b*). Starting with F_z, we suggest dividing the integration domain into the part located forward of the maximal width, and the part located aft of it. For the first part, we keep the integration order as in (C 7*a*); for the second part we keep it as in (C 7*b*). Thus,

$$F_z = \rho v \int_{-s_0}^{s_0} \mathrm{d}y \int_{x_{\mathrm{LE}}(y)}^{0} \frac{\partial\mu(x,\,y)}{\partial x}\,\mathrm{d}x$$

$$+ \rho v \int_{0}^{x_+} \mathrm{d}x \int_{s(x)}^{s(x)} \frac{\partial\mu(x,\,y)}{\partial x}\,\mathrm{d}y. \tag{C 17}$$

Noting that μ vanishes on the leading edge by (C 13), integration by parts in the first term readily yields

$$F_z = \rho v \int_{-s_0}^{s_0} \mu(0,\, y)\mathrm{d}y + \rho v \int_0^{x_+} \mathrm{d}x \int_{s(x)}^{s(x)} \frac{\partial \mu(x,\, y)}{\partial x}\mathrm{d}y. \tag{C 18}$$

Upon substituting (C 13) and (C 16) it becomes

$$F_z = \pi\rho v\, v_\perp(0) s_0^2 + \pi\rho v \int_0^{x_+} s^2(x) \frac{\mathrm{d}v_\perp(x)}{\mathrm{d}x}\mathrm{d}x. \tag{C 19}$$

By following the same steps with (C 8*a*) and (C 8*b*) one should find no difficulty in obtaining

$$M = \pi\rho v \int_{x_-}^{0} v_\perp(x) s^2(x)\mathrm{d}x - \pi\rho v \int_0^{x_+} x \frac{\mathrm{d}v_\perp(x)}{\mathrm{d}x} s^2(x)\mathrm{d}x \tag{C 20}$$

for the respective couple.

Consider now a particular case of a pseudo-elliptic wing with outline specified by

$$s(x) = \begin{cases} s_0\sqrt{1 - x^2/x_-^2}, & x \text{ in } (x_-, 0], \\ s_0\sqrt{1 - x^2/x_+^2}, & x \text{ in } (0, x_+), \end{cases} \tag{C 21}$$

and the camber specified by

$$f = \frac{4f_0}{c^2}(x_+ - x)(x - x_-). \tag{C 22}$$

With these, (C 19) and (3.9), respectively, yield

$$F_z = \frac{1}{2}\rho v^2 S\left(\frac{\pi A}{2}\alpha + 2\pi A \frac{f_0}{c}\left(1 - \frac{2x_+}{3c}\right)\right) \tag{C 23}$$

and

$$M = \frac{1}{2}\rho v^2 Sc\left(-\frac{\pi A}{3}\frac{x_-}{c}\alpha - \pi A \frac{2f_0}{c}\left(\frac{x_+}{c} + \frac{x_-(2x_+ - x_-)}{6c^2} - \frac{x_+^2}{2c^2}\right)\right). \tag{C 24}$$

For an elliptic wing ($x_+ = -x_- = c/2$), these further reduce to

$$F_z = \frac{1}{2}\rho v^2 S\left(\frac{\pi A}{2}\alpha + \frac{4\pi A}{3}\frac{f_0}{c}\right) \tag{C 25}$$

and

$$M = \frac{1}{2}\rho v^2 Sc\left(\frac{\pi A}{6}\alpha - \frac{\pi A}{2}\frac{f_0}{c}\right). \tag{C 26}$$

By definition, M is a couple about the y-axis, or, simply, about the widest point along the wing. It can be used to refer to any other point along the wing using a simple translation. For example, the couple M_0 about a point situated on the x-axis at the distance x_0 aft of the widest point is $M_0 = M + F_z x_0$. Two particular reference points are of interest. One is the centre of effort—a point where the couple vanishes. The other is the aerodynamic centre—a point where the couple is independent of the angle of attack. The former is located at

$$x_{\mathrm{CE}} = -\frac{M}{F_z} = -c\frac{\alpha - 3(f_0/c)}{3\alpha + 8(f_0/c)}; \tag{C 27}$$

the latter is located at

$$x_{\mathrm{AC}} = -\frac{\partial M/\partial\alpha}{\partial F_z/\partial\alpha} = -\frac{c}{3}. \tag{C 28}$$

For a cambered wing, i.e. the wing with $f_0 \neq 0$, the centre of effort moves considerably with the angle of attack, changing from three-eighths of the chord aft of the widest point at the zero angle of attack to one-third of the chord forward of the widest point at high angles of attack. The aerodynamic centre, on the other hand, is fixed at one-third of the chord forward of the widest point.

For future reference, we note that the couple about the aerodynamic centre is

$$M_{\mathrm{AC}} = M + x_{\mathrm{AC}} F_z = \frac{1}{2}\rho v^2 Sc\left(-\pi A \frac{17}{18}\frac{f_0}{c}\right). \tag{C 29}$$

It is obviously negative for a positive camber. Equations (C 25) and (C 29) were the basis for equations (3.7) and (3.8) in the text.

REFERENCES

Ashley H. & Landahl, M. 1985 *Aerodynamics of wings and bodies*, pp. 91–93, 122–123. New York, NY: Dover.

Bardi, J. & Marques, C. A. 2007 Taxonomic re-description of the Portuguese man-of-war, *Physalia physalis* (Cnidaria, Hydrozoa, Siphonophorae, Cystonectae) from Brazil, Iheringia. *Sér. Zool.* **97**, 425–433.

Batchelor, G. K. 1990 *An introduction to fluid dynamics*, pp. 314, 341. Cambridge, UK: Cambridge University Press.

Bisplinghoff, R. L., Ashley, H., & Halfman, R. L. 1996 *Aeroelasticity*, pp. 217, 219, 244–248. Mineola, NY: Dover.

Davenport, J. 2005 Swimbladder volume and body density in an armored benthic fish, the streaked gurnard. *J. Fish Biol.* **55**, 527–541. (doi:10.1111/j.1095-8649.1999.tb00697.x)

Francis, L. 1991 Sailing downwind: aerodynamic performance of the *Velella* sail. *J. Exp. Biol.* **158**, 117–132.

Hoerner, S. F. 1965 *Fluid dynamic drag*, p. 13.20. Albuquerque, NM: Hoerner Fluid Dynamics.

Madin, L. P. 1988 Feeding behavior of tentaculate predators: *In situ* observation and a conceptual model. *Bull. Mar. Sci.* **43**, 413–429.

Milne-Thomson, L. M. 1996 *Theoretical hydrodynamics*, pp. 135, 219–220, 5th edn. New York, NY: Dover.

Purcell, J. E. 1997 Pelagic cnidarians and ctenophores as predators: selective predation, feeding rates and effects on prey populations. *Annales de l'Institut Océanographique* **73**, 125–137.

Raymer, D. P. 1992 *Aircraft design: a conceptual approach*, pp. 279–281. Washington, DC: AIAA, Inc.

Torres, G. E. & Mueller, T. J. 2001 Aerodynamic characteristics of low-aspect-ratio wings at low Reynolds numbers. In *Fixed and flapping wing aerodynamics for micro air vehicles applications* (ed. T. J. Mueller), pp. 115–141. Reston, VA: AIAA, Inc.

Totton, A. K. & Mackie, G. O. 1960 Studies on *Physalia physalis*. *Discovery reports 30*, pp. 301–408. Cambridge, UK: Cambridge University Press.